DNA-Mediated Wirelike Clusters of Silver Nanoparticles: An Ultrasensitive SERS Substrate

Dipanwita Majumdar,[†] Achintya Singha,*,[†] Prasanna Kumar Mondal,[‡] and Subrata Kundu*,[§]

[†]Department of Physics, Bose Institute, 93/1, Acharya Prafulla Chandra Road, Kolkata 700009, India

[‡]Astroparticle Physics and Cosmology Division, Saha Institute of Nuclear Physics, 1/AF, Bidhannagar, Kolkata 700064, India

[§]Electrochemical Materials Science (ECMS) Division, CSIR−Central Electrochemical Research Institute (CECRI), Karaikudi 630006, India

ABSTRACT: Stable metal nanoclusters (NCs) with uniform interior nanogaps reproducibly offer a highly robust substrate for surface-enhanced Raman scattering (SERS) because of the presence of abundant hot spots on their surface. The synthesis of such an SERS substrate by a simple route is a challenging task. Here, we have synthesized a highly stable wirelike cluster of silver nanoparticles (Ag-NPs) with an interparticle gap of ~1.7 ± 0.2 nm using deoxyribonucleic acid (DNA) as the template by exploiting an easy and inexpensive chemical route. The red shift in the surface plasmon resonance (SPR) band of Ag-NCs compared to SPR of a single Ag-NP confirms the strong interplasmonic interaction. Methylene Blue (MB) is used as a representative Raman probe to study the SERS effect of the NCs. The SERS measurements reveal that uniform, reproducible, and strong Raman signals were observed up to the single-molecule level. The intensity of the Raman signal is not highly dependent on the polarization of the excitation laser. The DNA-based Ag-NCs as a substrate show better isotropic behavior for their SERS intensity compared to the dimer, as confirmed from both the experimental and theoretical simulation results. We believe that in the future the DNA-based Ag-NCs might be useful as a potential SERS substrate for ultrasensitive trace detection, biomolecular assays, NP-based photothermal therapeutics, and a few other technologically important fields.

KEYWORDS: *DNA templated silver nanocluesters, SERS, high enhancement factor, polarization study*
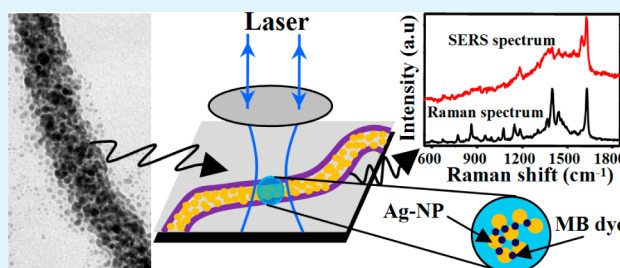
1. INTRODUCTION

Surface-enhanced Raman scattering (SERS) is a surface-sensitive technique that enhances the Raman signal of molecules adsorbed on rough metal surfaces by a factor of 10^{13} to 10^{15}, which empowers Raman spectroscopy as a powerful tool for the identification of trace amounts of chemical and biological species.[1−7] It is well known that the detection at the single-molecule level is the ultimate sensitivity desired for many areas of research such as biosensing, analytical chemistry, and biomedicine.[8,9] The localized electromagnetic (EM) field, which is usually taken to be proportional to the fourth power of the ratio between the local electric field and the incident field, originating from the resonant coupling of the incident light with surface plasmons, dominates to enhance the Raman signal in the SERS phenomenon.[10−17] Single metal nanoparticle (NP) typically do not provide enough enhancement of the Raman signal.[10] The plasmonic coupling effects at the nanometer gap junctions of the aggregated noble-metal particles (known as hot spots) provide an intensively localized electromagnetic field, which enables us to detect Raman active molecules adsorbed at the hot spots with single-molecule sensitivity.[10,18−25] However, the poor reproducibility of hot SERS-active NPs caused by inhomogeneous aggregation limitted the use of the SERS substrate for the in vivo bioimaging and in situ monitoring of biological processes.[10]

Therefore, a lot of efforts have been focused on the study of the impact of the different parameters and properties of the nanostructured metal substrates to enhance their SERS efficiency.[11,26,27] Recent studies showed that the gap between metallic nanostructures plays an important role to increase the SERS efficiency.[28−30] Many sophisticated techniques like focused-ion-beam, optical, and electron-beam lithography have been used to prepare SERS substrates with a uniform particle size and tunable gap between the particles.[31−34] However, most of the techniques are expensive, and it is not easy to reach an interparticle gap of less than 5 nm.[4] In practice, interparticle gaps within 2 nm experience a significant field-enhancement effect.[35] It is reported that the self-assembled structures of NPs can significantly reduce the interparticle gap, resulting in good sensitivity in SERS.[36] The exciting prospects of utilizing self-assembled nanostructures for application in various types of fundamental and applied studies have been reported.[36] Moreover, the self-assembled Ag-NPs show good sensitivity and specificity as a potential SERS substrate by exhibiting their utility for multiplexed lab-on-a-chip devices.[36] Recently, a few other studies highlighted the importance of the

**Scheme 1. Schematic Presentation of the Synthesis of Ag-NCs on DNA[a]**
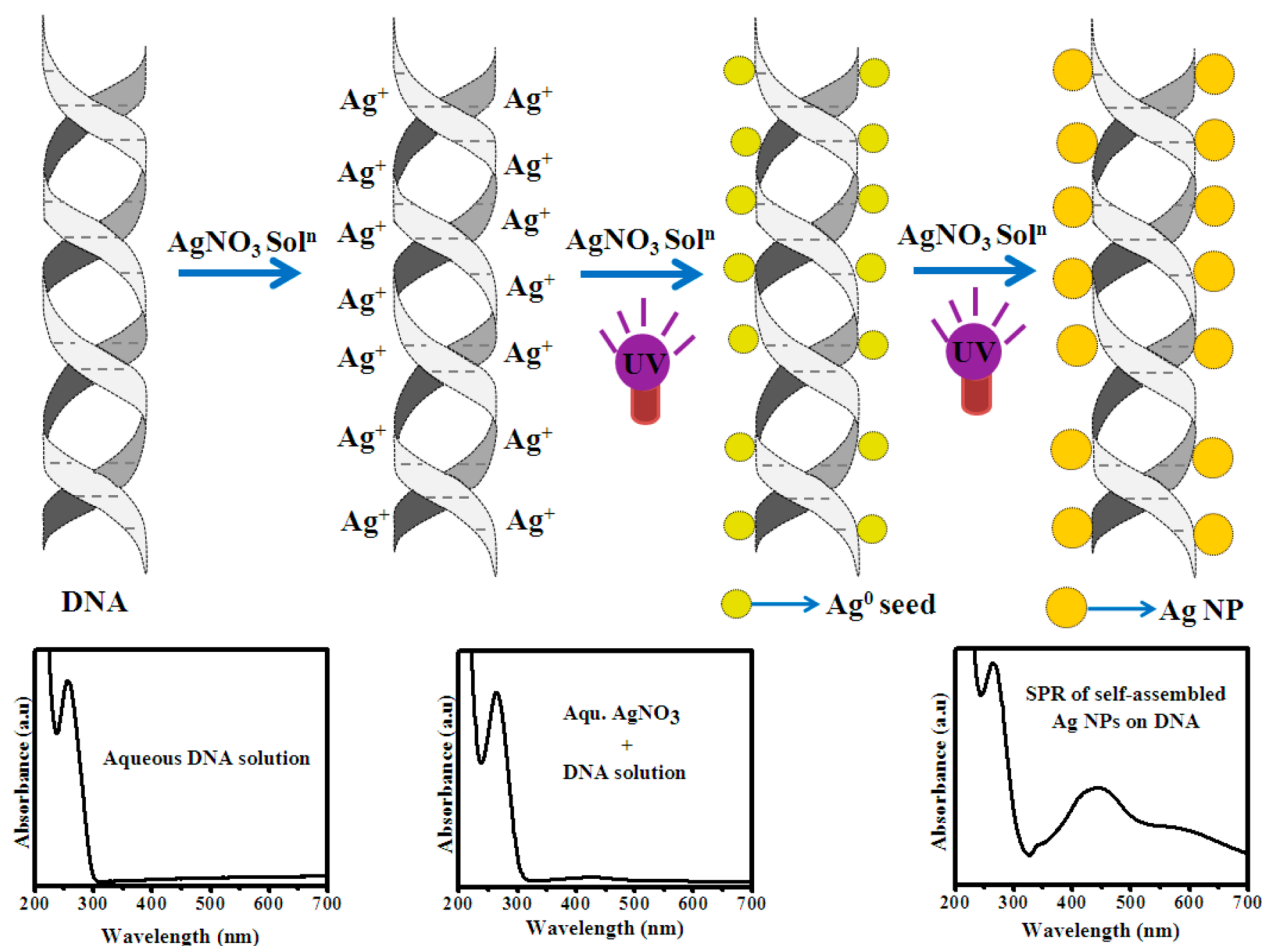
[a]UV−vis absorption spectra at three different stages are shown in the lower panel.

self-assembled structure of metal NPs (either gold or silver) for SERS studies.[37−39]

The conjugation of NPs with biomolecules yields ordered architectures that show promising features in different aspects.[39,40] Biomolecules have been successfully demonstrated to have templating capabilities for a number of nanoscale materials. Among the different biomolecules investigated for templating purposes, deoxyribonucleic acid (DNA) has been used as an inexpensive, well-characterized, controllable, and easily adaptable material whose physical properties can be explored to build inorganic nanostructures.[40−42] It is known that double-stranded DNA molecules have a diameter of ∼2 to 3 nm and the length can be varied on the micrometer scale level. Because of this large aspect ratio, DNA can be used as a superb platform for the construction of nanoscale assemblies. Moreover, the intermolecular interactions in DNA are reliably predicted, and their versatile chemical structure makes them an effective genetic material for programmed self-assembly.[43,44] There are several reports where researchers assembled NPs into DNA for different applications.[45−47] Fischler and Simon highlighted a short review where they suggested that the combination of DNA with NPs can generate a complex nanoarchitecture that can be potentially applicable for future technologies.[48] Moreover, it is important to note that in molecular plasmonic studies for lab-on-a-chip devices as well as molecular detections using SERS technique, DNA and metal (mainly gold and silver) particles are most commonly employed. Therefore, the synthesis of suitable SERS substrate in an easy and reproducible way with a narrow interparticle gap is extremely desirable to obtain a highly sensitive SERS signal, which is necessary for single-molecule detection.

Here, we have used a simple and inexpensive method to fabricate self-assembled wirelike Ag nano clusters (Ag-NCs) in a DNA template. Methylene Blue (MB) was used as a representative Raman probe to study the SERS effect of the nanoclusters (NCs) junctions. Highly stable, uniform, and reproducible SERS signals have been observed at up to a picomolar (pM) concentration of the dye. The enhancement factor (EF) is greater than 10^8, which is sufficient for the detection of single molecules. The polarization-dependent SERS study revealed that the intensity of the Raman signal is not highly dependent on the incident polarization. DNA-based Ag-NCs as the substrate showed better isotropic behavior for SERS intensity compared to the dimer, as confirmed from both the experimental and theoretical simulation results. The methodology reported here could lead to a uniform platform for the fabrication of a low-cost substrate to generate a new class of nanoprobes that might overcome the issues of low cross sections, signal reproducibility, quantification, and enhanced sensitivity in SERS. Moreover, the present methodology might be useful for various applications like ultrasensitive trace detection, biomolecular assays, nanoparticles-based photo-thermal therapeutics, and others.

7799

dx.doi.org/10.1021/am402448j | ACS Appl. Mater. Interfaces 2013, 5, 7798−7807
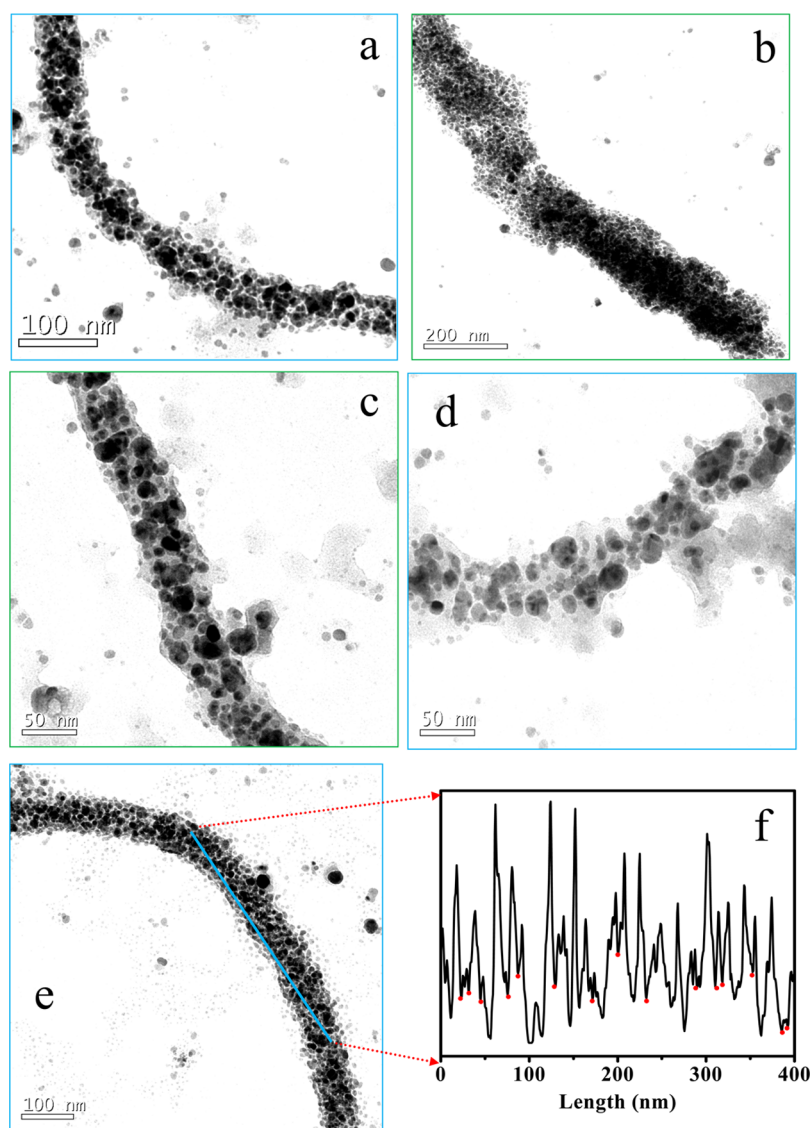
Figure 1. (a−e) TEM images of the DNA-templated wirelike Ag-NCs at different magnifications from different parts of the sample. The line profile of the selected region of panel e is shown in panel f. The hot spots are indicated by red dots.

2. EXPERIMENTAL SECTION

2.1. Reagents. Silver nitrate (AgNO$_3$, 99.99%, analytical grade) and Tris-EDTA buffer solution were purchased from Sigma-Aldrich, India and used as received. Double-stranded salmon testes DNA with an average size of ∼48 502 bp (base pairs) was purchased from Sigma and stored at 4 °C. The dye, methylene blue (C$_{16}$H$_{18}$N$_3$SCl; MB), was purchased from Loba Chemic Pvt. Ltd., India. Ultrapure distilled water (UPD) was used for the entire synthesis process and during the other experiments.

2.2. Preparation of Self-Assembled Ag-NCs on DNA. An AgNO$_3$ stock solution (10^{-2} M) was prepared, covered with a black paper, and stored in the dark to protect it from sunlight. A stock solution of DNA (60 μg/mL) was prepared by mixing a proper amount of DNA with Tris-EDTA buffer solution using UPD water. The solution containing the DNA was stirred using a magnetic stirrer for about 1 day to obtain a homogeneous solution of DNA in water. A measured volume of the AgNO$_3$ solution was mixed with the measured DNA solution, and the resulting solution mixture was placed under UV light at a wavelength of 260 nm for about 3 h. After the completion of the reaction, the solution became light-yellowish to yellowish-green (depending on the concentration ratio of DNA with Ag(I) ions), which confirmed the formation of Ag-NPs. The formation

of Ag-NPs was further confirmed from the SPR bands in the UV−vis spectrum.

2.3. Preparation of Samples for SERS Studies. A wide range of MB solutions having different concentrations (1 × 10^{-6} to 1 × 10^{-12} M) were prepared for the SERS measurements. The concentration of the Ag-NCs remained the same for all of the MB solutions at different concentrations. The measurements were carried out both in the solution phase and for dried samples. The dried samples were prepared by dropping the incubated solution of MB and Ag-NCs on a silicon substrate and allowing it to evaporate in a vacuum desiccator overnight.

2.4. Instruments Used for Various Characterizations. UV−vis spectroscopy was carried out using a Lambda-25 PerkinElmer spectrophotometer. TEM analysis was done using a Tecnai TEM instrument (Tecnai G2 F20, FEI) with an accelerating voltage of 200 kV to determine the particle size, shape, and morphology. The Raman scattering experiments were performed using a micro-Raman set up consisting of a spectrometer (model Lab RAM HR, Jobin Yvon) and a Peltier-cooled charge-coupled-device (CCD) detector. An air-cooled argon ion (Ar$^+$) laser with a wavelength of 488 nm was used as the excitation light source, and a 100× objective with a numerical aperture (NA) of 0.9 was used to get the laser spot diameter of ∼0.7 μm.

3. RESULTS AND DISCUSSION

The UV−vis spectra at various stages of the synthesis process of the Ag-NCs in DNA are shown in the lower panel of Scheme 1. A clear aqueous solution of DNA showed a λ_{max} at ~260 nm resulting from the absorption by the aromatic bases in the DNA, as shown in the left spectrum of the lower panel of Scheme 1. Upon mixing the aqueous AgNO₃ solution with the DNA solution, a weak hump was observed with an absorption maxima at ~420 nm (middle spectrum of the lower panel of Scheme 1) in addition to the parent DNA peak because of the instantaneous formation of the DNA−Ag⁺ complex. After continuous UV exposure of the solution mixture containing the DNA−Ag⁺ complex, a strong peak centered at around 440 nm appeared in addition to the parent DNA peak, as shown in the right spectrum of the lower panel of Scheme 1. This new peak at 440 nm is attributed to the surface plasmon resonance (SPR) of the Ag-NCs.[49−52] TEM analyses were performed to confirm the formation of Ag-NCs and to determine their size, shape, and morphology. Wirelike Ag-NCs were formed along the length of the DNA, as shown in Figure 1a−e at different magnifications from the different parts of the sample. The average diameter of the Ag particles is 17 ± 3 nm. The line profile of the image contrast for the selected region of Figure 1e is shown in Figure 1f. The sharp drop in contrast is due to the presence of a hollow gap between the NPs. The average gap between the individual NPs (indicated by red spot in Figure 1f) is estimated from the line profile to be ~1.7 ± 0.2 nm. In this narrow gap, the red shift of the SPR peak of Ag-NCs from individual Ag-NPs is due to the interaction of the induced dipoles.[53,54] In the simulation part of this work, discussed later, the detailed effect of the dipole interactions is elaborated upon.
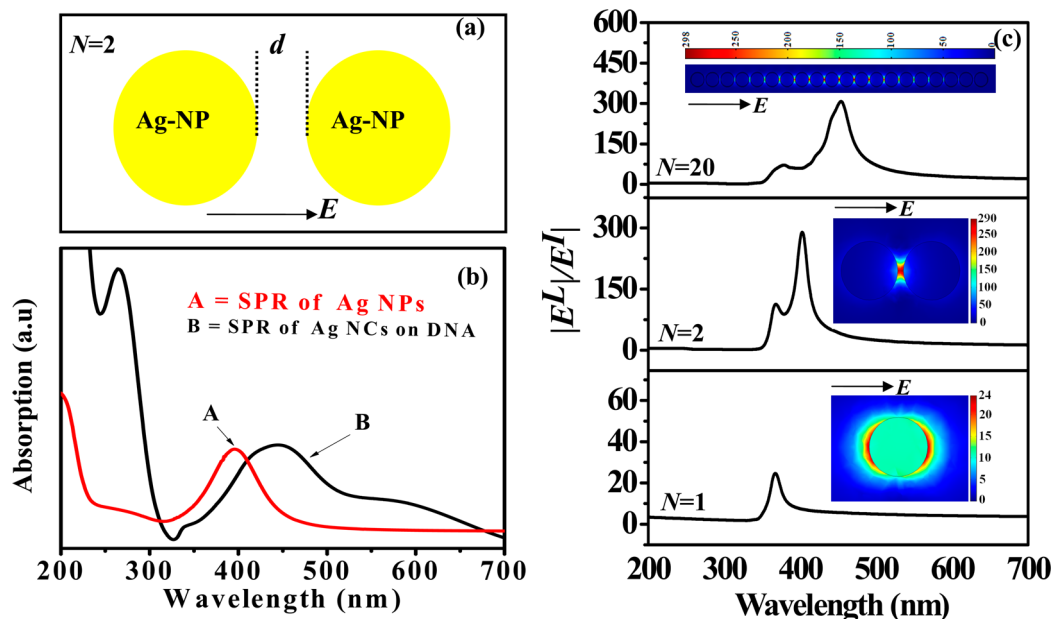
The formation mechanism of the Ag-NCs on DNA is shown in the upper panel of Scheme 1. Initially, after the addition of the Ag(I) ions to DNA, they form an instantaneous DNA−Ag(I) complex by embedding the Ag ions inside the double helix of the DNA. In the presence of continuous UV irradiation, the DNA−Ag(I) complex gets reduced, forming the Ag(0) particles that grow onto the DNA chain. Therefore, both the presence of DNA and UV light are crucial for the formation of Ag-NCs. It is well known that DNA has a negatively charged phosphate backbone and also has a chainlike structure, which gives rise to stabilized Ag-NCs with a definite morphology. Previously, Kundu et al. synthesized electrically conductive CdS nanowires in the presence of DNA and UV light and observed that DNA plays a major role in the formation of uniform nanowires.[55] Here, in our study, the positively charged Ag(I) ions initially bind with the negatively charged DNA molecules because of the electrostatic interactions and formed a stable DNA−Ag(I) complex, which can be confirmed from the shift in the absorption bands (middle spectrum of the lower panel of Scheme 1) compared to that of pure DNA. Now, in the presence of continuous UV light, the Ag(I) ions attached to DNA get reduced and form Ag(0) particles. Therefore, both the presence of DNA and UV lights are important for the synthesis of Ag-NPs. Here, DNA plays a dual role: first, it reduces the Ag(I) to Ag(0), and then the Ag(0) particles get stabilized along the DNA chain, probably via the nitrogen-containing base molecules present in DNA. The formation of Ag−nitrogen bonds was further confirmed from the FT−IR analysis (data not shown) by comparing pure DNA and DNA-templated Ag-NPs. The reducing capability of DNA in the presence of UV light can be explained as follows. In DNA,

hydroxyl group is present in the deoxyribose sugar. It was reported earlier that the presence of hydroxyl group in some organic compounds can reduce metal ions to metal NPs during UV irradiation.[56,57] In the presence of UV irradiation, the hydroxyl group breaks down to generate radical species, solvated electrons, or singlet oxygen species that are used during the reduction of metal ions to metal (0). In our proposed reaction, we also assume that the radical or singlet oxygen species probably play a major role in the reduction of Ag(I) to Ag(0).The reduction capability of DNA resulting from the presence of the hydroxyl group can be further proven by one control experiment. Instead of DNA, we used a negatively charged surfactant, sodium dodecyl sulfate (SDS), which was unable to generate any Ag particles on our proposed time scale under the same experimental conditions because of the lack of hydroxyl group on its structure. We also checked the specific role of UV light in our synthesis process. It was observed that in the absence of UV light no Ag-NPs were formed on our experimental time scale. Moreover, although we exposed the sample to UV light at 360 nm (away from the DNA absorption peak at 260 nm), we were unable to detect the Ag-NPs on the basis of the characteristic SPR peak and color of the solution on our experimental time scale. Therefore, these control experiments confirm that both the presence of DNA and UV light are crucial for the formation of self-assembled Ag-NCs on DNA chains. We observed that the formation of the DNA−Ag⁺ complex was instantaneous and 3 h of UV exposure was sufficient for the complete formation of the Ag-NPs. A longer exposure time (4−7 h) causes the agglomeration of the Ag-NPs in DNA, which gets precipitated in the solution, as confirmed from the TEM analysis (data not shown). During the synthesis, the preformed Ag(0) particle acts as a catalyst for the reduction of the remaining Ag(I) ions in solution, and finally all of the Ag(I) ions get reduced on the DNA and generate the self-assembled Ag-NCs on the DNA chains. We believe that the reduction mechanism of all of the Ag(I) ions proceeds via the 'autocatalytic growth' route where once a metal atom is evolved as a nucleation center it can act as a catalyst for the reduction of the remaining metal ions present in the solution via autocatalysis.[58] In our case, the Ag colloids were finally formed by the reduction of Ag ions with DNA via the transient intermediate formation of Ag clusters. At the initial stage of colloid formation, metal atoms were produced, which subsequently agglomerate and generate the colloidal particles.

To understand the experimental SERS results discussed later, we have simulated the induced electromagnetic (EM) field for the case of a linear and a 2D cluster of Ag-NPs. Our SERS substrate is more complicated than the model we used for the calculation because of the clusters of many particles. It is reported earlier that the quantitative result of SERS changes with the shape and size of the cluster, but the qualitative picture remains same, in particular in terms of the physics and characteristics of the hot spots.[59] As the major part of the EM enhancement is mainly due to the hot spots at the gap between two interacting NPs, the complicated structure of the cluster can be considerd to be a collection of dimers.

In classical theory, EM enhancement is caused by the amplification of the electric field resulting from the coupling between the light and the surface plasmons of the metal particles.[12,13] The EM field enhancement factor, M^{EM}, can be expressed as[12,13]

$$M^{EM} = [E^{L}(\nu_{I})/E^{I}(\nu_{I})]^2 \ [E^{L}(\nu_{I} - \nu_{S})/E^{I}(\nu_{I} - \nu_{S})]^2$$

7801

dx.doi.org/10.1021/am402448j | ACS Appl. Mater. Interfaces 2013, 5, 7798−7807

Figure 2. (a) Model for the calculation of the induced EM field at the middle of the gap (d) between two identical Ag particles of radius R. (b) SPR band of an isolated Ag-NP (A, red curve) of diameter of 17 nm and Ag-NCs (B, black curve) constituted by Ag-NPs of an average diameter of 17 nm. (c) Wevelength-dependent field enhancement at the surface of a single Ag particle ($N = 1$) as well as at the middle of the gap of a dimer and a linear array of 20 NPs. (Here, E indicates the direction of polarization of the incident EM field.)

E^I and E^L are the incident electric field and the total local electric field in the presence of the metal particle, respectively. ν_I and ν_s are the incident and scattered laser frequencies, respectively. If $\nu_s \ll \nu_I$, then the above equation can be written as:

$$M^{EM} = [E^L(\nu_I)/E^I(\nu_I)]^4$$

The total local electric field can be written as the sum of the incident field and the induced field given by

$$E^L(r_m, \nu) = E^I(r_m, \nu) + E^{ind}(r_m, \nu)$$

where $E^{ind}(r_m, \nu) = \int G(r_m, r) \, \rho(\nu, r) \, E^L(r, \nu) dr$. Here, $G(r_m, r)$ is the tensor Green function relating points r_m and r. To get the gross but essential understanding of the EM enhancement, we have calculated the local field numerically. A 3D finite element method has been applied for the calculation.[60,61] We have used the COMSOL Multiphysics program for the entire simulation study.[62]

The schematic diagram of a dimer formed by two identical metal particles of radius R and gap d is shown in Figure 2a. In the DNA-mediated wirelike Ag-NCs, the particles are oriented along the length of the wire. We consider the system to be a collection of many dimers in a linear way. We also consider a system in which the dimers are arranged in a 2D plane (because there are few particles along the width of the wires, as can be seen from TEM images). For the simulation, we have used a particle size ($2R$) of 17 nm and an interparticle gap (d) of 1.7 nm. The empirical dielectric function of Ag has been taken from Johnson and Christy.[63] The EM enhancement is highly sensitive to the dieletric constant of the surrounding medium. An increase in the medium dielectric constant increases the electromagnetic coupling between noble-metal nanoparticles of a coupled system.[64] The Ag-NPs in our sample are attached to the DNA. We assume that 25% of the surface area of the NPs is covered by DNA. We have determined the effective dielectric

constant of the medium, which is a mixture of air and DNA, by using Maxwell−Garnett formalism.[30]

$$\varepsilon_{eff} = \varepsilon_0 \frac{\varepsilon_{DNA}(1 + 2\theta) + 2\varepsilon_0(1 - \theta)}{\varepsilon_{DNA}(1 - \theta) + \varepsilon_0(2 + \theta)}$$

ε_{eff} is the effective dielectric constant of the mixture of air and DNA. ε_0 and ε_{DNA} are the dielectric constants of air and DNA, respectively. θ is the fraction of surface area of the NPs covered by DNA. Taking the dielectric constant of air (ε_0) = 1 and DNA (ε_{DNA}) = 2.53 from literature,[65] we have calculated the wavelength-dependent EM enhancement in (i) an isolated Ag NP (N = 1), (ii) a dimer (N = 2), and (iii) a linear array of 20 NPs. The polarization of the incident field is along the direction of the linear array. Figure 2c shows the calculated results. The result indicates that the plasmon coupling effect in a coupled system not only shows the red shift in the optical resonance but also shows the higher field enhancement as compared to an isolated particle. We also observed the appearance of higher-order multipolar resonance at a lower wavelength in coupled systems. The position of the resonance enhancement for N = 1 at around 370 nm is red shifted to 455 nm for N = 20, which agrees well with the SPR peak of the isolated NP and Ag-NC (as shown in Figure 2b). This result indicates that the linear array of 20 NPs provides a qualitative picture of our Ag-NCs in terms of EM field enhancement. We would also like to mention here that the presence of DNA on the surface of the NPs increases the medium dielectric constant with respect to air. The increase of the medium dielectric constant reduces the Coulomb dielectric constant, resulting in the increase of the dipole moment compared to air. A net increase in the plasmon coupling strength occurs with the increase in the dipole moment. We have observed that the presence of DNA in the medium results in an EM field enhancement that is ∼3 times greater than the air medium.

We have also calculated induced EM field enhancement profile for a dimer (Figure 3a), a linear array containing 20 NPs
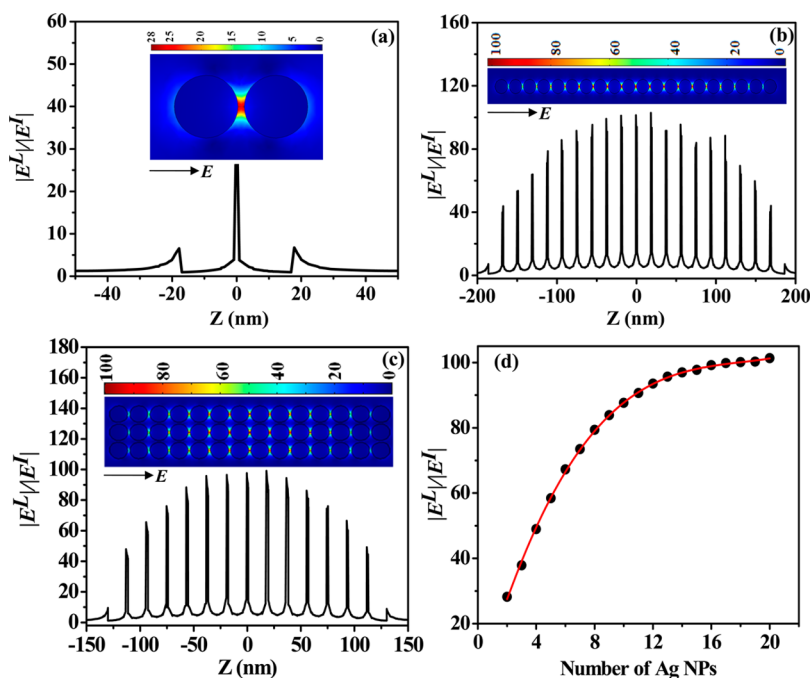
Figure 3. Induced EM field enhancement profile along the axis of a (a) dimer, (b) linear array consisting of 20 particles, and (c) 2D 14 × 3 array. In all the cases, the diameter of the Ag-NP is 17 nm, and the interparticle gap is 1.7 nm. (Here, E indicates the direction of the polarization of the incident EM field.) (d) Induced EM field enhancement as a function of the number of particles.

(Figure 3b), and a 2D array (Figure 3c) using an excitation wavelength of 488 nm (because the SERS measurements have been done using 488 nm). The magnitude of the maximum induced EM field increases up to 14 NPs and shows a saturating behavior if we further increase the number of particles (Figure 3d). Our substrate is not a linear array, rather it is a complicated orientation of the NPs both along the length and width. To model this system, we consider a 2D array. Because of the limitation of computer power, we used an array with 14 NPs along the length (for this number of particles, the saturation of EM field enhancement occurs) and 3 NPs along the width. For incident polarization along the length of the array, the value of the induced EM field is the same as the linear array of 14 NPs. Therefore, in the zero-polarization angle there is no effect of the NPs along the width. The axis of our SERS substrate is not always parallel to the incident polarization. The effect of the polarization angle has been discussed later. The magnitude of the maximum induced EM field amplification for 20 NPs is 100, and the corresponding EF value is 1×10^8.

The normal Raman spectrum of an aqueous solution of MB (1×10^{-3} M) is presented in Figure 4. The characteristic bands of MB are observed at 1630, 1591, 1544, 1442, 1399, and 1188 cm^{-1}. The bands at 1630 and 1591 cm^{-1} are related to stretching vibration of the C−C ring.[66] The Raman lines at around 1544, 1442, 1399, and 1188 cm^{-1} can be assigned to the asymmetric stretching of C−C, asymmetric stretching of C−N, in-plane ring deformation of C−H, and stretching of C−N, respectively.[66] The time-dependent SERS measurements have been performed on a 1×10^{-6} M MB solution immediately after mixing with Ag-NCs. The cationic MB molecules are efficiently adsorbed on the negatively charged silver surface. Figure 5a shows the contour plot of the time-dependent SERS intensity of MB Raman bands. The spectra corresponding to the lines on the contour plot are shown in Figure 5b. The acquisition time for each spectrum was 1 min. The intensity of
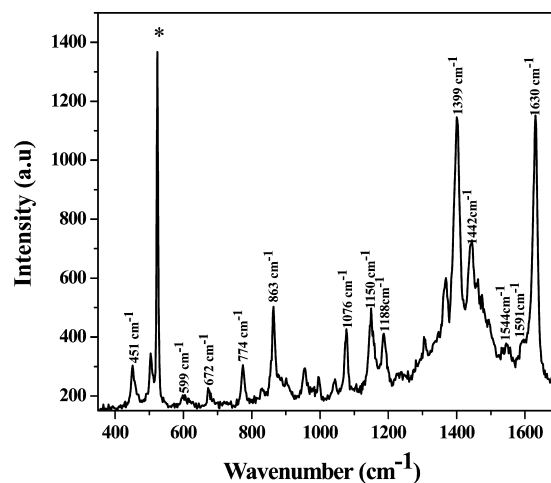

Figure 4. Raman spectrum of MB at a concentration of 10^{-3} M. The asterisk (*)-marked peak is from the Si substrate.
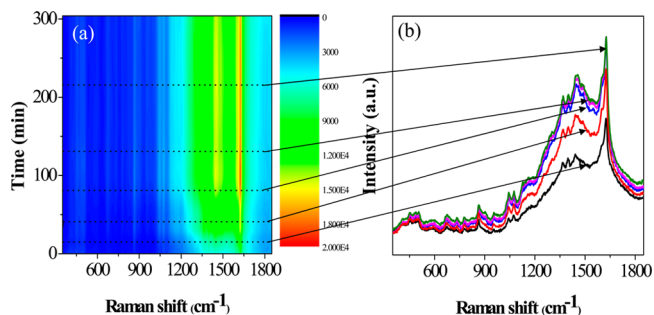
Figure 5. (a) Contour plot of the SERS intensity of MB (1×10^{-6} M) with increasing incubation time. (b) Spectra corresponding to the lines on the contour plot.

the characteristic Raman peaks of MB increased concomitantly with the increase in the incubation time. The strongest and most stable signals were obtained after 1 h of incubation. Therefore, the subsequent SERS measurements have been performed after 1 h of aging the MB solution with Ag-NCs to avoid fluctuation in the intensity of the Raman modes during the formation of a stable MB−Ag-NPs complex. The stability of the signal was sustained even after 3 months.

To explore the utility of the DNA-based Ag-NCs as an efficient SERS substrate, the concentration-dependent SERS measurements have been performed on the mixtures of Ag-NCs with MB solutions having concentrations of 1×10^{-6}, 1×10^{-8}, and 1×10^{-12} M. The measurements have been performed with the dried samples under similar reaction conditions. Figure 6 shows the UV-vis spectra of the reagents
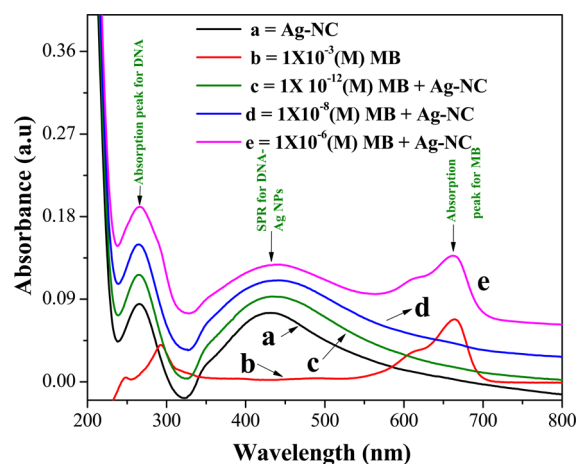
Figure 6. UV−vis spectra of Ag-NCs (a, black color), MB (b, red color), and the mixture of Ag-NCs with MB at concentrations of 1×10^{-12} M (c, olive color), 1×10^{-8} M (d, blue color), and 1×10^{-6} M (e, magenta color).

used for making the SERS samples (Ag-NCs, and MB) and the mixtures of Ag-NCs with MB at different concentrations. The broadening and shift of the plasmon resonance peak of the Ag-NCs confirms the adsorption of MB molecules on the surface of the NCs.[56,57] The schematic representation for the SERS measurements in the back-scattering configuration is shown in Figure 7a. The recorded SERS spectra at various concentrations are shown in Figure 7b. Aqueous Ag-NCs and the bare MB solution (1×10^{-5} M) do not show any Raman bands, as can be seen in the black (A) and green (C) curves in Figure 7b. However, the characteristic Raman modes of MB were observed in the SERS spectra at concentrations of less than 1×10^{-5} M. More importantly, the Raman bands were observed even for concentration as low as the picomolar level. The intensity of the Raman signals decreases with the decrease in the concentration of the dye molecules, which is consistent with an earlier report.[30] To get a quantitative idea from our measurements, the EF values have been calculated using the following formula

$$EF = (I_{SERS}/N_{SERS})/(I_{ref}/N_{ref})$$

where I_{ref} (I_{SERS}) and N_{ref} (N_{SERS}) are the intensity of the normal Raman mode (SERS) and the number of molecules in the reference sample (SERS sample), respectively. The values of N_{ref} (at 10^{-3} M) and N_{SERS} (at 10^{-12} M) within the area covered by laser light (diameter of the laser spot ∼0.7 μm) are

calculated to be ∼7×10^9 and ∼1, respectively. The EF values at 1625, 1595, 1376, and 1184 cm^{-1} are in the range between 10^8 and 10^{10}. The experimental EF values are higher than the theoretically simulated results. This is satisfactory because the chemical enhancement and surface-roughness effects were not included in our calculation. Those effects are expected to increase the Raman intensity in actual experiments.

The optical stability and the reproducibility of our SERS substrate have been studied by time-dependent Raman measurements. The acquisition time for a single spectrum was 1 s, and we collected Raman spectra continuously for 200 s. Figure 8 shows the Raman spectra collected at positive integer multiples (1, 2, 3, ..., 10) of 10 s. Other spectra are not presented because of the difficulty in accommodating them in one figure. Highly uniform and reproducible Raman signals were observed throughout the measurements. This result indicates that the substrate is highly stable and shows excellent reproducibility.

Thus far, we have discussed the efficiency of the SERS substrate in terms of EF and stability. However, the understanding of the polarization-dependent study could eventually be used to extend the application of the SERS substrate. Figure 9 panels a and b shows the calculated polarization-dependent induced EM field for a dimer and a 4×4 array. In the dimer, the enhancement of the local EM field is strongly dependent on the polarization of the incident field, and the enhancement is at a maximum when the polarization is in the direction of the dimer axis.[67] In the 4×4 array, the polarization-dependent induced electric field is more isotropic with respect to the isolated dimer. The presence of hot spots for any polarization could be a possible reason for such a behavior.

The polarization-dependent response of our SERS substrate for MB bands at 1595 and 1624 cm^{-1} are shown in Figure 9c. Surprisingly, the intensity variation of the modes with the polarization angle agrees well with the simulation. We interpret such polarization-dependent quasi-isotropic behavior to be a result of entangled electromagnetic coupling between several particles, as shown in the color plot of Figure 9b. Therefore, in the present process, we were able to synthesize a highly stable wirelike cluster of Ag-NPs with an interparticle gap of ∼1.7 ± 0.2 nm using DNA as the template by exploiting an inexpensive chemical route that shows uniform, reproducible, and strong Raman signals up to the single-molecule level. The experimental results were compared with theoretical simulation, and were found to be in good agreement. We believe that in future the newly developed SERS substrate will be useful for ultrasensitive trace detection, biomolecular assays, NPs-based photothermal therapeutics, and other technologically important fields.

4. CONCLUSIONS

We have successfully synthesized highly dense and wirelike Ag-NCs with an average particle size of 17 ± 3 nm using UV irradiation of a solution mixture containing DNA and silver nitrate by exploiting a simple wet-chemical route. The average gap between the individual Ag-NPs is ∼1.7 ± 0.2 nm, as observed from TEM analysis. The Ag-NCs in DNA were shown to act as a potential substrate for the SERS experiment. The presence of DNA not only plays an important role for the formation of the Ag-NCs but also remarkably enhances the SERS signals. The quantitative estimation of the EF values from the experimental results is within the range of 10^8 to 10^{10},

7804

dx.doi.org/10.1021/am402448j | ACS Appl. Mater. Interfaces 2013, 5, 7798−7807
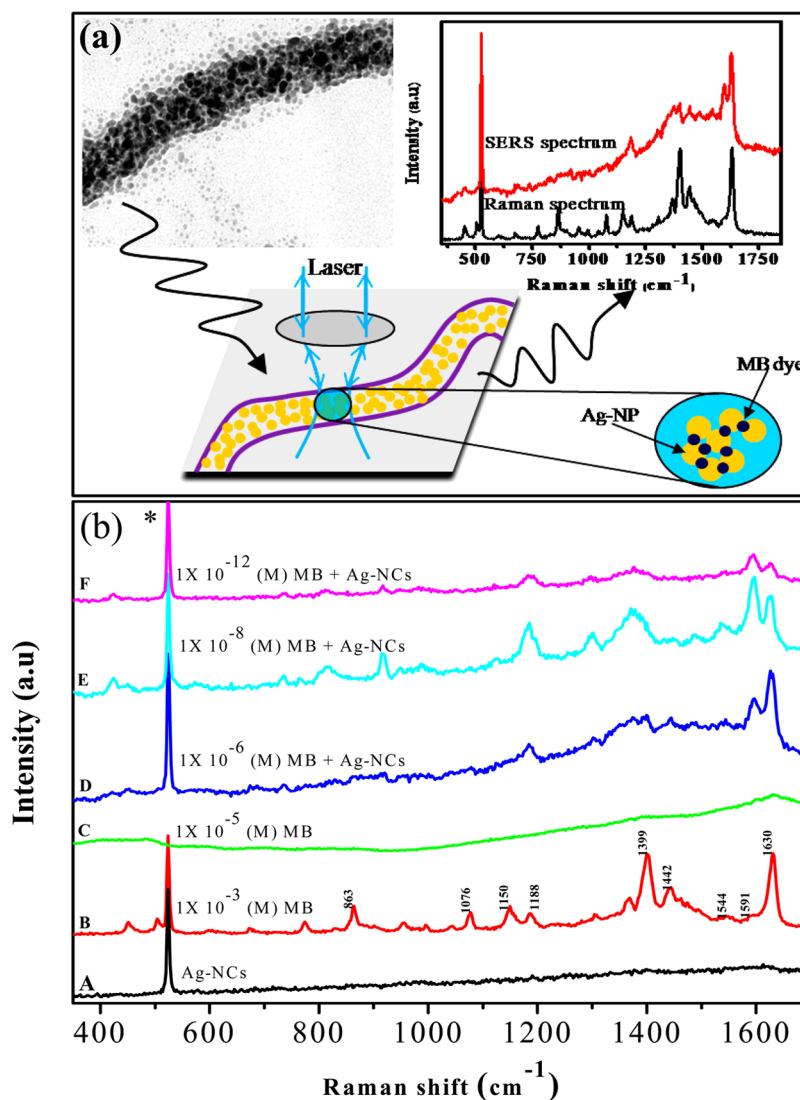
Figure 7. (a) Schematic presentation of the SERS measurements. (b) Raman spectra of Ag-NCs (A, black) and MB at concentrations of 1×10^{-3} M (B, red) and 1×10^{-5} M (C, green) as well as SERS spectra of MB at concentrations of 1×10^{-6} M (D, blue), 1×10^{-8} M (E, cyan), and 1×10^{-12} M (F, purple), respectively. The asterisk (*)-marked peak is from the Si substrate.
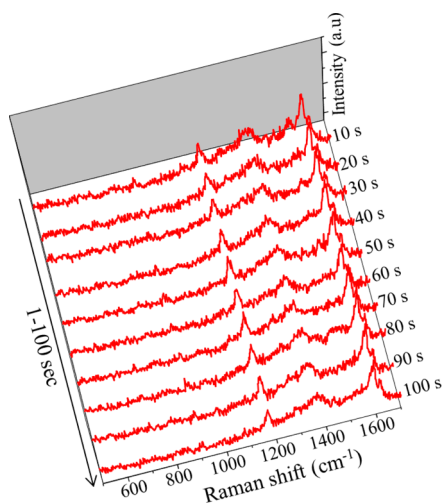
Figure 8. Time-dependent SERS spectra of MB at a concentration of 1×10^{-12} M. The numbers on the right represent the time at which the spectra were taken.

which is sufficient to detect a single molecule. The intensity of the SERS signals remains almost unaltered even after 3 months of aging, and the time-dependent uniform SERS response signifies the high stability and excellent reproducibility of our samples. Because of the complicated orientation of the Ag-NPs in the clusters, the polarization response showed better isotropic behavior for SERS intensity compared to the dimer. The experimental results were found to match nicely with the theoretical simulation data. Our study showed a new fabrication method for a low-cost, highly sensitive SERS substrate. Therefore, in the future, we believe that the DNA-based synthesis technique might be useful for the formation of a series of new nanogap structures for other materials with uniform morphology that might act as a potential SERS substrate for label-free biomedical sensing, Raman imaging, and NPs-based photothermal therapeutics.
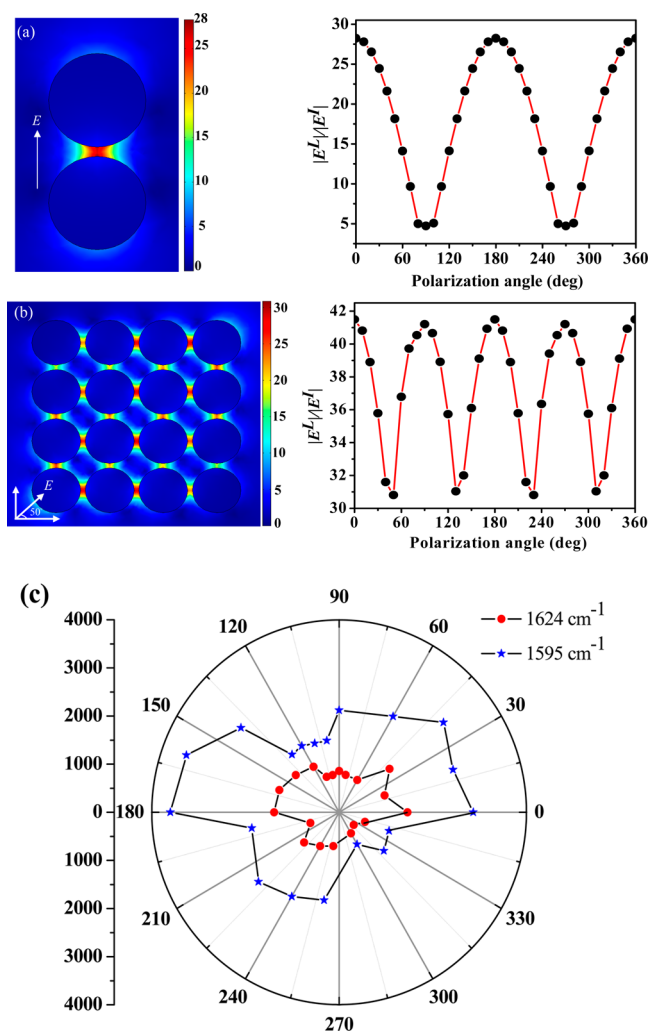
Figure 9. (a, b) Polarization-angle dependent EM field for a dimer and a cluster consisting of 16 Ag-NPs, respectively. The particle size, gap, and wavelength of the incident light are 17, 1.7, and 488 nm, respectively. (Here, E indicates the direction of polarization of the incident EM field.) (c) Polar plot of the intensity of the MB Raman bands at 1595 and 1624 cm^{-1}.

■ AUTHOR INFORMATION

Corresponding Author
*E-mail: achintya@jcbose.ac.in (A.S.), Phone: + 91 33 23031177, Fax: + 91 33 23506790. E-mail: skundu@cecri.res.in (S.K.), Phone: + 91 4565 241487, Fax: + 91 4565 227713.

Notes
The authors declare no competing financial interest.

■ ACKNOWLEDGMENTS

■ REFERENCES

(1) Nie, S. M.; Emory, S. R. *Science* **1997**, *275*, 1102−1106.
(2) Kneipp, K.; Wang, Y.; Kneipp, H.; Perelman, L. T.; Itzkan, I.; Dasari, R.; Feld, M. S. *Phys. Rev. Lett.* **1997**, *78*, 1667−1670.
(3) Kneipp, K.; Kneipp, H.; Deinum, G.; Itzkan, I.; Dasari, R. R.; Feld, M. S. *Appl. Spectrosc.* **1998**, *52*, 175−178.
(4) Liang, H.; Li, Z.; Wang, W.; Wu, Y.; Xu, H. *Adv. Mater.* **2009**, *21*, 4614−4618.
(5) Kneipp, K.; Kneipp, H.; Manoharan, R.; Hanlon, E. B.; Itzkan, I.; Dasari, R. R.; Feld, M. S. *Appl. Spectrosc.* **1998**, *52*, 1493−1497.
(6) Deckert, V.; Zeisel, D.; Zenobi, R.; Vo-Dinh, T. *Anal. Chem.* **1998**, *70*, 2646−2650.
(7) Zeisel, D.; Deckert, V.; Zenobi, R.; Vo-Dinh, T. *Chem. Phys. Lett.* **1998**, *283*, 381−385.
(8) Xie, X. S.; Trautman, J. K. *Annu. Rev. Phys. Chem.* **1998**, *49*, 441−480.
(9) Kulzer, F.; Orrit, M. *Annu. Rev. Phys. Chem.* **2004**, *55*, 585−611.
(10) Li, Q.; Jiang, Y.; Han, R.; Zhong, X.; Liu, S.; Li, Z. Y.; Sha, Y.; Xu, D. *Small* **2013**, *9*, 927−932.
(11) Emory, S. R.; Haskins, W. E.; Nie, S. *J. Am. Chem. Soc.* **1998**, *120*, 8009−8010.
(12) Xu, H.; Aizpurua, J.; Käll, M.; Apell, P. *Phys. Rev. E* **2000**, *62*, 4318−4324.
(13) Xu, H.; Bjerneld, E. J.; Käll, M.; Börjesson, L. *Phys. Rev. Lett.* **2000**, *83*, 4357−4360.
(14) Moskovits, M. *J. Raman Spectrosc.* **2005**, *36*, 485−496.
(15) Bosnick, K. A.; Jiang, J.; Brus, L. E. *J. Phys. Chem. B* **2002**, *106*, 8096−8099.
(16) Otto, A. *J. Raman Spectrosc.* **2002**, *33*, 593−598.
(17) Camden, J. P.; Dieringer, J. A.; Wang, Y.; Masiello, D. J.; Marks, L. D.; Schatz, G. C.; Van Duyne, R. P. *J. Am. Chem. Soc.* **2008**, *130*, 12616−12617.
(18) Yang, L.; Yan, B.; Premasiri, W. R.; Ziegler, L. D.; Negro, L. D.; Reinhard, B. M. *Adv. Funct. Mater.* **2010**, *20*, 2619−2628.
(19) Moskovits, M. *Rev. Mod. Phys.* **1985**, *57*, 783−826.
(20) Michaels, A. M.; Jiang, J.; Brus, L. *J. Phys. Chem. B* **2000**, *104*, 11965−11971.
(21) Tian, Z.-Q.; Ren, B.; Wu, D.-Y. *J. Phys. Chem. B* **2002**, *106*, 9463−9483.
(22) Tao, A.; Kim, F.; Hess, C.; Goldberger, J.; He, R.; Sun, Y.; Xia, Y.; Yang, P. *Nano Lett.* **2003**, *3*, 1229−1233.
(23) Willets, K. A.; Van Duyne, R. P. *Annu. Rev. Phys. Chem.* **2007**, *58*, 267−297.
(24) Le, F.; Brandl, D. W.; Urzhumov, Y. A.; Wang, H.; Kundu, J.; Halas, N. J.; Aizpurua, J.; Nordlander, P. *ACS Nano* **2008**, *2*, 707−718.
(25) García-Vidal, F. J.; Pendry, J. B. *Phys. Rev. Lett.* **1996**, *77*, 1163−1166.
(26) McFarland, A. D.; Young, M. A.; Dieringer, J. A.; Van Duyne, R. P. *J. Phys. Chem. B* **2005**, *109*, 11279−11285.
(27) Kundu, S. *J. Mater. Chem. C* **2013**, *1*, 831−842.
(28) Li, J. F.; Huang, Y. F.; Ding, Y.; Yang, Z. L.; Li, S. B.; Zhou, X. S.; Fan, F. R.; Zhang, W.; Zhou, Z. Y.; De, Y. W. *Nature* **2010**, *464*, 392−395.
(29) Cho, W. J.; Kim, Y.; Kim, J. K. *ACS Nano* **2012**, *6*, 249−255.
(30) Lim, D.-K.; Jeon, K.-S.; Hwang, J.-H.; Kim, H.; Kwon, H.; Suh, Y. D.; Nam, J.-M. *Nat. Nanotechnol.* **2011**, *6*, 452−460.
(31) Ebbesen, T. W.; Lezec, H. J.; Ghaemi, H. F.; Thio, T.; Wolff, P. A. *Nature* **1998**, *391*, 667−669.
(32) Tseng, A. A. *Small* **2005**, *1*, 924−939.
(33) Altewischer, E.; van Exter, M. P.; Woerdman, J. P. *Nature* **2002**, *418*, 304−306.
(34) Abu Hatab, N. A.; Oran, J. M.; Sepaniak, M. J. *ACS Nano* **2008**, *2*, 377−385.
(35) Kneipp, K.; Kneipp, H.; Itzkan, I.; Dasari, R. R.; Feld, M. S. *J. Phys.: Condens. Matter* **2002**, *14*, R597−R624.
(36) Tao, A. R. *Pure Appl. Chem.* **2009**, *81*, 61−71.
(37) Clayton, D. A.; Benoist, D. M.; Zhu, Y.; Pan, S. *ACS Nano* **2010**, *4*, 2363−2373.

(38) Huang, T.; Meng, F.; Qi, L. *J. Phys. Chem. C* **2009**, *113*, 13636−13642.

(39) Strelau, K. K.; Weber, K.; Möller, R.; Fritzsche, W.; Popp, J. *Proc. SPIE* **2010**, *7715*, 771514-1−771514-7.

(40) Kundu, S.; Liang, H. *Langmuir* **2008**, *24*, 9668−9674.

(41) Lee, S. W.; Mao, C. B.; Flynn, C. E.; Belcher, A. M. *Science* **2002**, *296*, 892−895.

(42) Mcmillan, R. A.; Paavola, C. D.; Howard, J.; Zaluzec, N. J.; Trent, J. D. *Nat. Mater.* **2002**, *1*, 247−252.

(43) Mirkin, C. A.; Letsinger, R. L.; Mucic, R. C.; Storhoff, J. J. *Nature* **1996**, *382*, 607−609.

(44) Braun, E.; Eichen, Y.; Sivan, U.; Ben-Yoseph, G. *Nature* **1998**, *391*, 775−778.

(45) Mirkin, C. A. *Inorg. Chem.* **2000**, *39*, 2258−2272.

(46) Monson, C. F.; Woolley, A. T. *Nano Lett.* **2003**, *3*, 359−363.

(47) Keren, K.; Krueger, M.; Gilad, R.; Ben-Yoseph, G.; Sivan, U.; Braun, E. *Science* **2002**, *297*, 72−75.

(48) Fischler, M.; Simon, U. *J. Mater. Chem.* **2009**, *19*, 1518−1523.

(49) Yu, D.; Yam, V. W. *J. Am. Chem. Soc.* **2004**, *126*, 13200−13201.

(50) Pal, T.; Sau, T. K.; Jana, N. R. *Langmuir* **1997**, *13*, 1481−1485.

(51) Kundu, S.; Wang, K.; Liang, H. *J. Phys. Chem. C* **2009**, *113*, 134−141.

(52) Singha, A.; Dasgupta, S.; Roy, A. *Biophys. Chem.* **2006**, *120*, 215−224.

(53) Zheng, Y.; Thai, T.; Reineck, P.; Qiu, L.; Guo, Y.; Bach, U. *Adv. Funct. Mater.* **2013**, *23*, 1519−1526.

(54) Hobro, A. J.; Lendl, B. In *Surface Enhanced Raman Spectroscopy: Analytical, Biophysical and Life Science Applications*; Schlucker, S., Ed.; Wiley-VCH: Weinheim, Germany, 2011; pp 1−37.

(55) Kundu, S.; Liang, H. *Adv. Mater.* **2008**, *20*, 826−831.

(56) Esumi, K.; Suzuki, A.; Aihara, N.; Usui, K.; Torigoe, K. *Langmuir* **1998**, *14*, 3157−3159.

(57) Kundu, S.; Wang, K.; Liang, H. *J. Phys. Chem. C* **2009**, *113*, 18570−18577.

(58) Henglein, A. *Chem. Rev.* **1989**, *89*, 1861−1873.

(59) Etchegoin, P. G.; Galloway, C.; Le Ru, E. C. *Phys. Chem. Chem. Phys.* **2006**, *8*, 2624−2628.

(60) Wustholz, K. L.; Henry, A. I.; McMahon, J. M.; Freeman, R. G.; Valley, N.; Piotti, M. E.; Natan, M. J.; Schatz, G. C.; Van Duyne, R. P. *J. Am. Chem. Soc.* **2010**, *132*, 10903−10910.

(61) Anil, K.; Kodali, A. K.; Llorad, X.; Bhargava, R. *Proc. Natl. Acad. Sci. U.S.A.* **2009**, *107*, 13620−16625.

(62) COMSOLAB, COMSOL, COMSOL MULTIPHYSICS, COMSOL Reaction Engineering Lab, and FEMLAB are registered trademarks of COMSOLAB. Other product or brand names are trademarks or registered trademarks of their respective holders. All rights reserved. 1998−2010.

(63) Johnson, P. B.; Christy, R. W. *Phys. Rev. B* **1972**, *6*, 4370−4379.

(64) Jain, P. K.; El-Sayed, M. A. *Nano Lett.* **2008**, *8*, 4347−4352.

(65) Inagaki, T.; Hamm, R. N.; Arakawa, E. T. *J. Chem. Phys.* **1974**, *61*, 4246−4250.

(66) Xiao, G. N.; Man, S. Q. *Chem. Phys. Lett.* **2007**, *447*, 305−309.

(67) Xu, H.; Kall, M. *ChemPhysChem* **2003**, *4*, 1001−1005.

■ NOTE ADDED AFTER ASAP PUBLICATION

This paper was published on the Web on August 14, 2013, with minor errors in two equations on the fifth page. The corrected version was reposted on August 16, 2013.